Asian Journal of Civil Engineering (2019) 20:1037–1048
https://doi.org/10.1007/s42107-019-00164-8

ORIGINAL PAPER

Behaviour of cold-formed steel built-up closed columns composed by angle profiles

G. Aruna[1] · S. Sukumar[2] · V. Karthika[3]

Received: 2 January 2019 / Accepted: 5 July 2019 / Published online: 15 July 2019

Abstract

This paper presents the experimental investigation of cold-formed built-up closed sections with intermediate web stiffeners under axial compression with hinged end conditions. The specimens were formed using two angle sections with edge and intermediate stiffeners, connected by self-tapping screws. Three series of tests were conducted by varying the width of the intermediate web element. Twelve columns were tested by varying the column length. The specimens were failed by local, flexural, and interaction of these buckling modes. Non-linear Finite-element Analysis (FEA) was carried out using ANSYS. FEA results were compared with the experimental results. It is observed that FEA results closely resemble to experimental results. An extensive parametric study was carried out using validated finite-element model by varying the cross-sectional geometries of cold-formed built-up closed section with intermediate stiffeners. The column strengths predicted from the FEA was compared with the design strengths calculated using the AISI specification of cold-formed steel structures. The reliability of the current design method was assessed by reliability analysis.

Keywords Columns · Distortional buckling · Finite-element analysis · Flexural buckling · Local buckling

List of symbols

W_f	Width of the flange element
W_1	Width of the top and bottom of the web element
W_2	Width of the inclined web element
W_3	Width of the intermediate stiffener of the web element
W_w	Width of the web
W_l	Width of the lip
θ	Angle of inclination
f_y	Yield stress
f_u	Ultimate stress
E	Young's modulus
P_n	Nominal axial strength
A_e	Effective area
F_n	Critical buckling stress
λ_c	Non-dimensional slenderness ratio
F_e	Least of the elastic flexural torsional and flexural–torsional buckling stress
σ_{FEA}	Ultimate compressive stress obtained by experiment
σ_{AISI}	Ultimate compressive stress obtained by AISI
β	Safety index (Reliability index)
ϕ	Resistance (Capacity) factor
DL	Dead load
LL	Live load
M_m	Mean value of the material factor
F_m	Mean value of the fabrication factor
V_m	Coefficient of variation of the material factor
V_F	Coefficient of variation of the fabrication factor
P_m	Mean value of σ_{FEA} to σ_{AISI} ratio
V_p	Coefficient of variation of σ_{FEA} to σ_{AISI} ratio
C_p	Correction factor in reliability analysis
FEA	Finite Element Analysis
AISI	American Iron Steel and Institute

✉ G. Aruna
aarunasree@gmail.com

S. Sukumar
sukumar_237@yahoo.co.in

V. Karthika
karthikadpm@gmail.com

[1] Department of Civil Engineering, CMR Institute of Technology, Hyderabad, India

[2] Department of Civil Engineering, Paavai College of Engineering, Namakkal, Tamil Nadu, India

[3] Department of Civil Engineering, Jai Shriram Group of Institution, Tiruppur, Tamil Nadu, India

Introduction

In recent years, the cold-formed steel structural members are widely used in building construction. The cold-formed steel members can be formed by press brake or bending brake operations. They are usually formed as open and built-up section. A lot of research is carried out on cold-formed open section by Young and Hancock (1992), Popovic et al. (1999), Dhanalakshmi and shanmugam (2001), Schafer (2002), Yan and Young (2002), Narayanan and Mahendran (2003), Elobody and Young (2005), Young and Ellobody (2007), Zhang et al. (2007) and Young and Chen (2008a). In addition, some research was carried out on cold-formed built-up section such as Stone and Laboube (2005), Sukumar et al. (2006), Young and Chen (2008b), Whittle and Ram seyer (2009), Reyes and Guzmanc (2011), Georgieva et al. (2012), Zhang and Young (2012), Piyawat et al. (2013), Yuanqi Li et al. (2014), Aruna et al. (2015), Ting et al. (2017), Fratamico et al. (2018), and Roy et al. (2018a, b, c, 2019). Very little research is carried out on cold-formed built-up closed I section formed by connecting two open channels back to back and box section formed by connecting the channel sections toe to toe. Still, many test data have not been reported on cold-formed steel built-up closed section formed by connecting two angle sections with edge and intermediate stiffeners.

This paper describes an experimental investigation on the compressive strength and behaviour of cold-formed built-up closed section with intermediate web stiffeners under hinged end conditions. Totally 12 specimens were tested by varying the column length. An accurate and reliable finite-element model was developed using ANSYS. The finite-element model was validated against the test results. The validated finite-element model was used for an extensive parametric study. The strength obtained from the finite-element analysis was compared with the design strengths calculated using AISI specification of cold-formed steel structures. The reliability of the current design equation on the cold-formed built-up closed section with intermediated stiffeners was also investigated.

Experimental investigation

Test specimens

The test specimens were formed by connecting two angle sections with intermediate web stiffeners using self-tapping screws. Figure 1 illustrates the typical cross section of built-up section. The nominal dimensions of the cross section such as width of the top and bottom web element

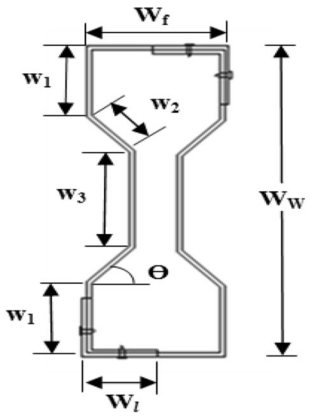

Fig. 1 Cross section of built-up closed section

(w_1), width of the inclined web element (w_2), width of the intermediate web element (w_3), width of the flange (W_f), width of the lip (W_l), and total width of the web (W_w) are presented in Table 1. The screws were arranged at a spacing of 200 mm and minimum edge distance of 20 mm, as shown in Fig. 2.

The test specimens were categorized into three series based on the width of the intermediate web element and the specimens were labelled, such that BC40, BC50, and BC60 accordingly. For example, the label "BC40L440", "BC" indicates the built-up closed section, "40" indicates the width of the intermediate web element, and the letter "L" indicates the nominal length of the specimen and follows by the digits "440" showing the length of the column.

Tensile coupon tests were conducted to obtain the material properties of the specimen. The coupon specimens were prepared according to IS 1608-2005 part I. Strain gauge was used to measure the longitudinal strain and the test results are listed in Table 2. Figure 3 shows the stress–strain behaviour for the specimen.

Experimental setup and operations

The column test was performed in a 1000 kN capacity self-straining loading frame. All the specimens were tested under axial compression with hinged end conditions (2015). Thick rubber gaskets were placed between the base plate and the platens (thick steel plate) to simulate the hinged–end conditions, at both supports (2006). The verticality of the specimen was also checked. The load was applied at the bottom end of the specimen through a hydraulic jack of 1000 kN capacity. A load cell was mounted above the hydraulic jack to measure the load increments. Three LVDTs were used two at the mid height, one on the flange and the other on the web to measure the lateral deflection and one at the bottom plate of the specimen to measure the axial shortening of the specimen. A data acquisition system was used to record the

Table 1 Nominal dimensions of the cross section

Specimen ID	Flange	Web				Lip	Angle	Thickness	Length
	W_f (mm)	W_w (mm)	W_1 (mm)	W_2 (mm)	W_3 (mm)	W_l (mm)	θ (deg)	T (mm)	L (mm)
BC40L440	50	130	30	21.2	40	15	45	1.6	440
BC40L840	50	130	30	21.2	40	15	45	1.6	840
BC40L1640	50	130	30	21.2	40	15	45	1.6	1640
BC40L2240	50	130	30	21.2	40	15	45	1.6	2240
BC50L440	50	140	30	21.2	50	15	45	1.6	440
BC50L840	50	140	30	21.2	50	15	45	1.6	840
BC50L1640	50	140	30	21.2	50	15	45	1.6	1640
BC50L2240	50	140	30	21.2	50	15	45	1.6	2240
BC60L440	50	150	30	21.2	60	15	45	1.6	440
BC60L840	50	150	30	21.2	60	15	45	1.6	840
BC60L1640	50	150	30	21.2	60	15	45	1.6	1640
BC60L2240	50	150	30	21.2	60	15	45	1.6	2240

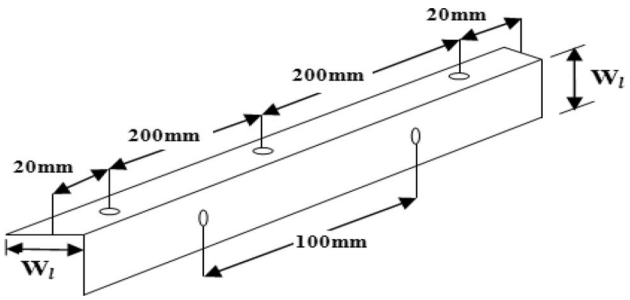

Fig. 2 Arrangements of screw spacing for 440 mm length of column

models for the subsequent non-linear buckling analysis. In the second stage, after incorporating the geometric imperfections, a non-linear buckling analysis was carried out using the arc-length method (2007). Centre line dimensions were used to model the cross section of the specimens.

Finite-element model

Shell 181 elements were used in the buckling analysis and structural mass 21 element was used to create the master node which has 6 degrees of freedom. 10 × 10 mm element size was used to model the specimens. The con-

Table 2 Tensile test results

Test specimen	Steel thickness T (mm)	Yield stress F_y (N/mm^2)	Ultimate stress F_u (N/mm^2)	Young's modulus E (N/mm^2)
1	1.6	272	356	2.03×10^5
2	1.6	271	340	2.04×10^5
3	1.6	273	352	2.04×10^5
Average		272	349	2.04×10^5

applied load and readings of the LVDT. The experimental setup is shown in Fig. 4.

Finite-element analysis

General

Finite-element analysis package ANSYS was used for the numerical investigation and it was carried out in two stages. In the first stage, an Eigen buckling analysis was carried out to establish the possible Eigen buckling modes of the specimen, which was used as initial geometric imperfection of the

nections between two angle sections were modelled by coupling the translational and rotational degree of freedoms of x, y, and z directions at the screw location. In FEA, the material behaviour was described by a bilinear stress–strain curve. The material properties were taken from the tensile test results such as average yield stress of the material 272 N/mm^2, young's modulus 2.04×10^5 N/mm^2, and tangent modulus as 2% of the young's modulus. The effect of residual stress on the ultimate load was considered to be negligible as recommended by Schaffer and Pekoz (1998). The strain hardening of the corners due to cold forming was neglected. The maximum initial

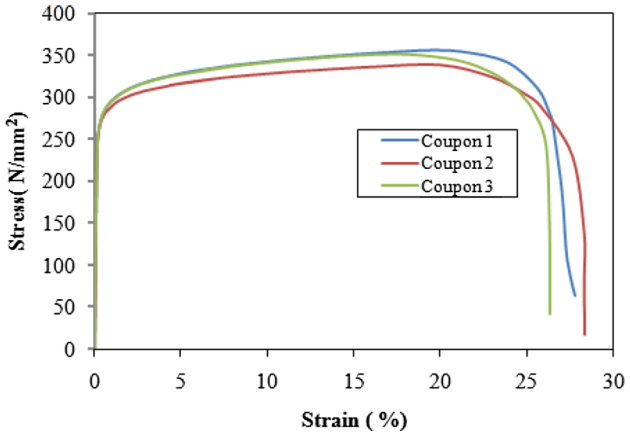

Fig. 3 Stress–strain behaviour for the specimen

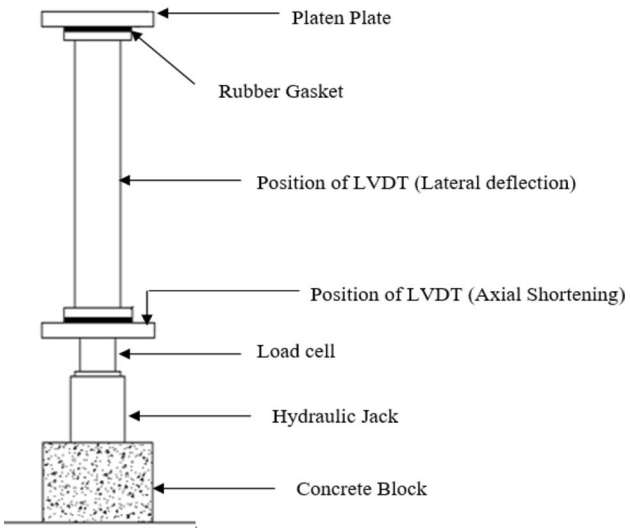

Fig. 4 Experimental setup

local and overall imperfection was taken as 0.25 times the thickness of the plate element (2002) and 1/1000 of the column length (AISC 2005), respectively. Super position of two possible least different eigen modes was factored by the magnitude of initial local and overall geometric imperfection. The loading end and reaction end were defined as master nodes, which were modelled at the centroid of the section. These master nodes were coupled to each node on the edge of the cross section. The load and boundary conditions were established to the master node. Rotation about *y*-axis and translations in both *x* and *z* directions were restrained at the top end and translation in three directions *x*, *y*, *z* and rotation about *y*-axis were restrained at the bottom. The modelling of screw connection and boundary conditions is shown in Fig. 5.

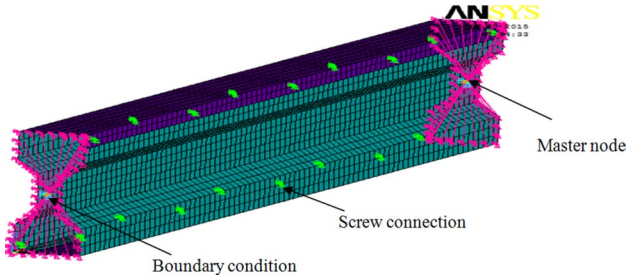

Fig. 5 Modeling of specimen

Validation of finite-element model

The finite-element analysis results were compared with the experimental results. The main aim of this comparison is to validate and ensure the accuracy of the finite-element analysis. The comparison of ultimate compressive stress and failure modes was obtained from the experimental and finite-element analysis is presented in Table 3. It shows that the FEA results were slightly higher than the experimental results. The mean value of $\sigma_{FEA}/\sigma_{EXP}$ ratio is 1.047 with the corresponding coefficient of variation of 0.019. The failure modes were local buckling and flexural buckling and interaction of local and flexural buckling. The local buckling was observed in the column of length of 440 mm. The interaction of local and flexural buckling was observed in 840 and 1640 mm length of the columns and flexural buckling was observed in 2240 mm length of the column. The comparison of axial compressive stress vs. axial shortening curve and axial compressive stress vs. lateral deflection curve of the specimens was obtained from the FEA and experiments are shown in Figs. 6, 7, 8, 9, 10, and 11. It shows that both column stiffness and behaviour reflects good agreement between experimental and finite-element results. The comparison of deformed shapes observed from the experimental and FEA for BC40L840, BC40L1640, and BC40L2240 is shown in Figs. 12, 13, and 14, respectively. It is shown that the deformed shapes of the specimens obtained from the FEA closely simulate the experimental deformed shapes.

Parametric study

FEA model was validated by the experimental results. It was shown that the FEA closely predicted the behaviour of stiffened built-up closed section. Hence, parametric study was carried out using validated finite-element model to investigate the effect of all influential parameters such as width of the top and bottom of the web element, width of the intermediate web element, width of the flange, width of the lip, and angle of the inclined web element. Totally, 60 specimens were taken for the parametric studies. Identification label

Table 3 Comparison between experiment and FEA results

Specimen ID	Experiment		FEA		$\sigma_{FEA}/\sigma_{EXP}$
	σ_{EXP} (N/mm^2)	Failure mode	σ_{FEA} (N/mm^2)	Failure mode	
BC40L440	257.71	L	268.34	L	1.041
BC40L840	236.32	L+F	249.38	L+F	1.055
BC40L1640	159.22	L+F	162.67	L+F	1.022
BC40L2240	96.34	F	103.08	F	1.070
BC50L440	255.18	L	267.53	L	1.048
BC50L840	235.00	L+F	248.04	L+F	1.055
BC50L1640	154.15	L+F	157.44	L+F	1.021
BC50L2240	96.63	F	99.52	F	1.030
BC60L440	259.43	L	264.56	L	1.020
BC60L840	233.79	L+F	246.54	L+F	1.055
BC60L1640	142.27	L+F	153.05	L+F	1.076
BC60L2240	89.81	F	96.12	F	1.070
Mean					1.047
Coefficient of variation					0.019

L local buckling, *F* flexural buckling

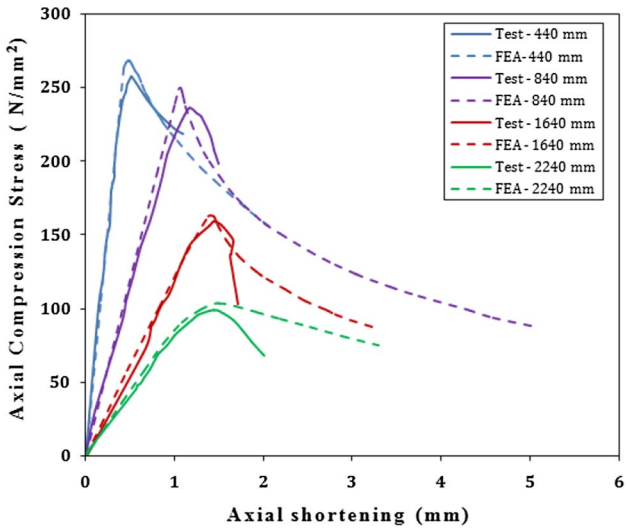

Fig. 6 Axial compressive stress vs. axial shortening curves for BC40 series

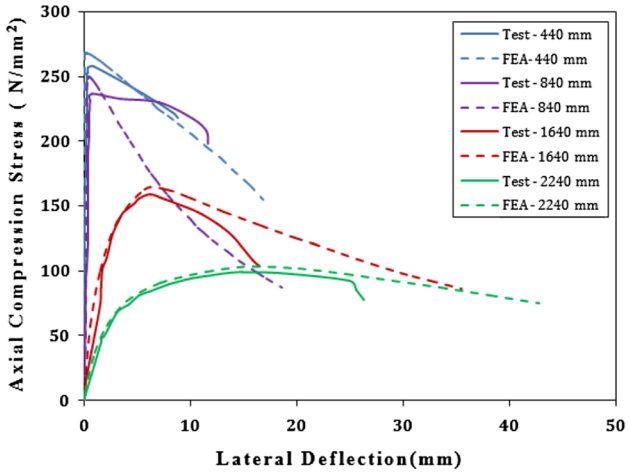

Fig. 7 Axial compressive stress vs. lateral deflection curves for BC40 series

of the specimen is shown in Fig. 15. For example, in the label, "TB30-I80-F50-L15-A45-440" defines the specimens as follows:

- "TB30" indicates the top and bottom of the web element with the width of 30 m (i.e., w_1).
- "I80" indicates the intermediate web element with the width of 80 mm (i.e., w_3).
- "F50" indicates the flange of the specimen with the width of 50 mm (i.e., W_f).
- "L15" indicates the lip of the specimen with the width of 15 mm (i.e., W_l).
- "A45" indicates the angle of inclined web element with an angle of 45°.
- "440" mean the column length of the specimen.

Design rule

The main design rules investigated in this study are that specified in the American Iron and Steel Institute (2007). The nominal axial strength P_n is calculated from the following design formula for concentrically loaded compression members using the AISI specifications:

$$P_n = A_e F_n, \quad (1)$$

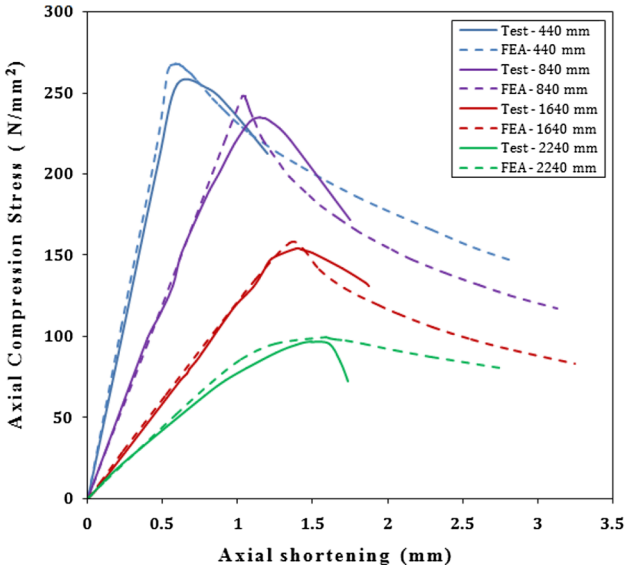

Fig. 8 Axial compressive stress vs. axial shortening curves for BC50 series

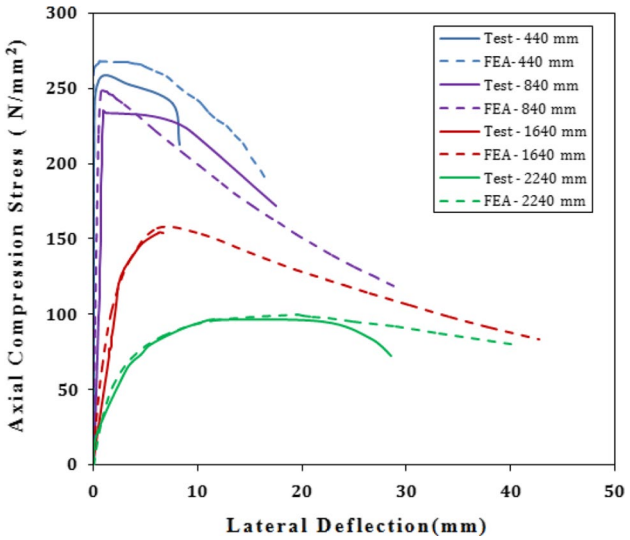

Fig. 9 Axial compressive stress vs. lateral deflection curves for BC50 series

where A_e is the effective area and F_n is the critical buckling stress.

The critical buckling stress F_n is calculated as

$$F_n = (0.658^{\lambda_c^2}) \quad \text{for } \lambda_c \le 1.5, \tag{2}$$

$$F_n = (0.877/\lambda_c^2) \quad \text{for } \lambda_c > 1.5, \tag{3}$$

where λc = non-dimensional slenderness ratio calculated as

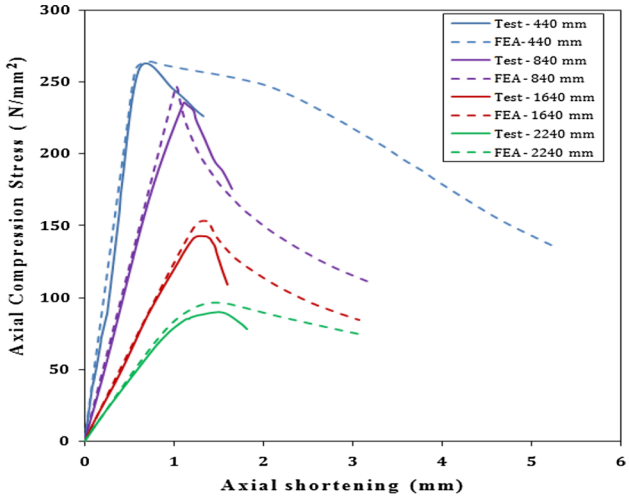

Fig. 10 Axial compressive stress vs. axial shortening curves for BC60 series

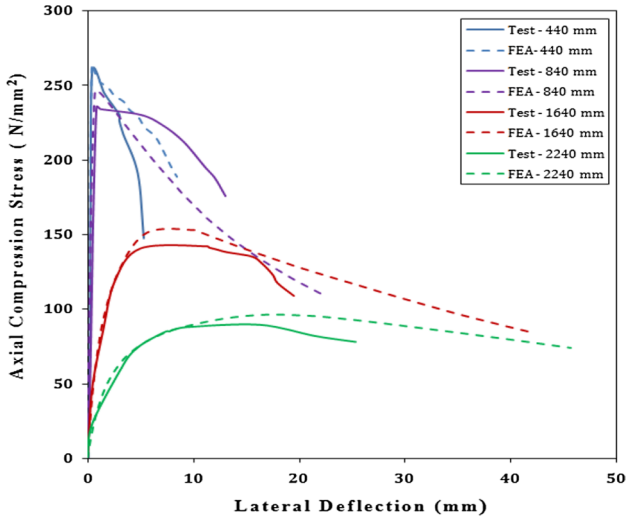

Fig. 11 Axial compressive stress vs. lateral deflection curves for BC60 series

$$\lambda_c = \sqrt{\frac{F_y}{F_e}},$$

where F_y is the yield stress which is equal to the 0.2% proof stress, F_e is the least of the elastic flexural, torsional, and flexural-torsional buckling stress determined in accordance with Sects. C 4.1.1–C 4.1.5 of the AISI Specification. The modified slenderness approach in Sect. D 1.2 of the AISI specification (described in Eq. 4) was used to calculate the critical elastic column buckling load for the built-up compression members:

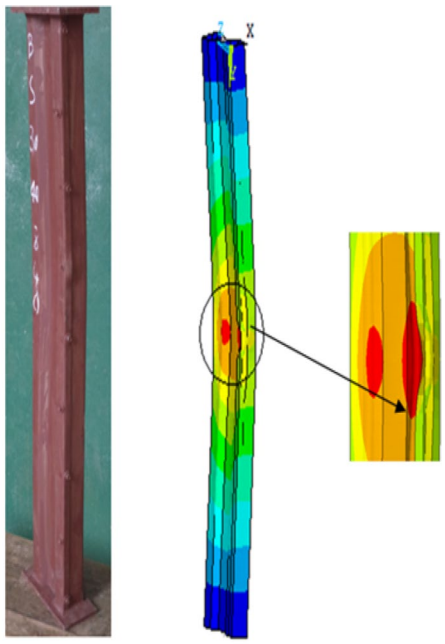

Fig. 12 Comparison of experimental and FEA-deformed shape for specimen BC40L840

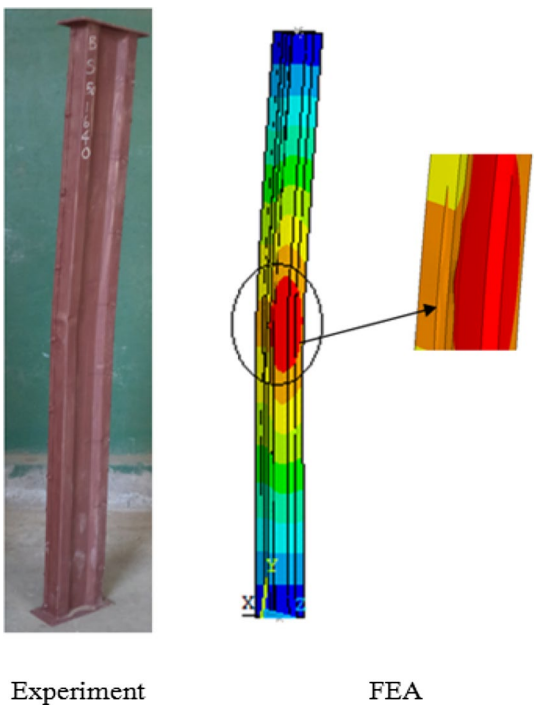

Fig. 13 Comparison of experimental and FEA-deformed shape for specimen BC40L1640

Fig. 14 Comparison of experimental and FEA-deformed shape for specimen BC40L2240

$$\left(\frac{KL}{r}\right)_m = \sqrt{\left(\frac{KL}{r}\right)_0^2 + \left(\frac{a}{r_i}\right)^2}, \tag{4}$$

where $\left(\frac{KL}{r}\right)_m$ is the modified slenderness ratio, $\left(\frac{KL}{r}\right)_o$ is the overall slenderness ratio of the entire section about built-up member axis, "a" is the intermediate fasterner spacing, and "r_i" is the minimum radii of gyration of full unreduced cross-sectional area of an individual shape in a built-up member.

Reliability analysis

The reliability of the current design method was evaluated using reliability analysis. A target reliability index (β) of 2.5 for cold-formed structural members is recommended by the

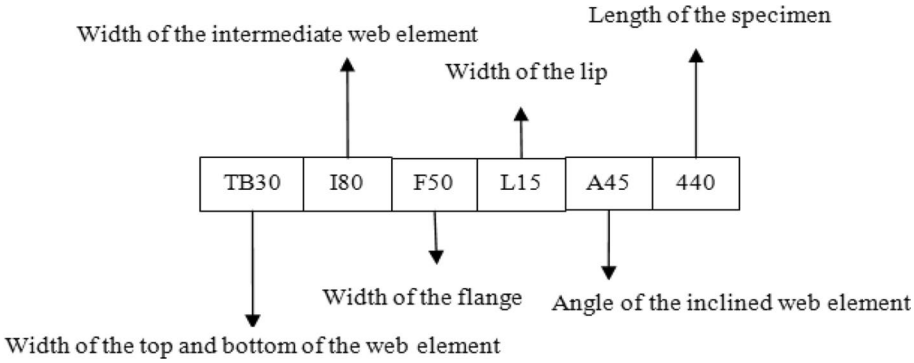

Fig. 15 Identification of the specimen

AISI Specification (2007). The resistance factor (ϕ) of 0.8 was used in the analysis as specified in the NAS Specification (2007) and AS/NZS Standard (AS/NZS 2005). A load combination of 1.2 DL + 1.6 LL as specified in the American Society of Civil Engineers Standard (2005) was used in the reliability analysis, where DL is the dead load and LL is the live load. The statistical parameters M_m, F_m, $V_{M,}$ and V_F are the mean values and coefficients of variation for material properties and fabrication variables. These values are obtained from Table Fl of the AISI Specification [2007] for concentrically loaded compression members, where $M_m = 1.10$, $F_m = 1.00$, $V_M = 0.10$, and $V_F = 0.05$. The statistical parameters P_m and V_P are the mean value and coefficient of variation of σ_{Exp} or $\sigma_{FEA}/\sigma_{AISI}$ ratio, as shown in Table 4. The correction factor C_p is used to account for the influence due to a small number of specimens.

Results and discussion

The parametric study was used to investigate the effect of all influential cross-sectional parameters on the strength and behaviour of cold-formed built-up closed section. Local buckling, distortional buckling, and flexural bulking, and interaction of local–distortional, local–flexural, and distortional–flexural buckling were observed from the FEA. Figures 16, 17, 18, 19, and 20 shows the comparison between the ultimate compressive stresses with width of the various elements.

As shown in Fig. 16, the ultimate compressive stress of the columns has closer values when the width increases from 30 to 80 and the compressive stress suddenly decreases beyond this width for the column length 440 mm and 840 mm except for the column length 1640 and 2240 mm. As shown in Fig. 17, the ultimate compressive stress decreases with an increase in the width of the intermediate web element for the all column length. As shown in Fig. 18, the ultimate compressive stress increase when the width of the flange is increase from 40 to 50 and slightly decrease beyond this width for the column length with 440 mm and 840 mm. However, the ultimate compressive stress is increase when the width of the flange is increase from 40 to 80 and the compressive stress suddenly decreases beyond this width for the column length with 1640 mm and 2240 mm. This indicates that the effect of flange width is dissimilar for different failure modes. As shown in Fig. 19, the ultimate compressive stresses have almost same for the lip width with 10, 15, and 30 mm. As shown in Fig. 20, the ultimate compressive stress of the columns has closer values when the angle of inclination increases from 30° to 60°, and beyond this angle, the stress is suddenly decrease for all the column length of the specimen. The parametric study results are concluded that 1. The width of the top and bottom of the web element, width of the intermediate web element, width of the flange, and angle of inclination of the web element having a significant effect on the strength and behaviour of the cold-formed built-up closed section. 2. Section with the lowest W/t ratio has more axial compressive resistance. 3. The variation of lip width does not affect the strength of built-up cold-formed closed columns. 4. The variation angle 30–60° does not influence the strength of built-up cold-formed closed columns.

The results obtained from the experiment and the results of the parametric study from FEA are compared with the nominal unfactored design strengths obtained using the AISI Specification are presented in Table 4. It was observed that, local buckling, flexural buckling was observed for the slenderness ratio ranges from 9.89 to 54.06, 63.21 to 168.56, respectively. Interaction of local–distortional, distortional–flexural, and local–flexural buckling was observed for the slenderness ratio ranges from 24.33 to 55.44, 45.42 to 46.71, and 33.11 to 109.39, respectively. The mean value of the (σ_{Exp} or $\sigma_{FEA}/\sigma_{AISI}$) ratio is 1.07, with the coefficient of variation (COV) of 0.081, and the corresponding values of β is 3.19. It is shown that the reliability index is greater than the target value of 2.5. Therefore, the column strengths predicted by the AISI predictions are conservative and reliable.

Table 4 Comparison of FEA results with design strength of cold-formed built-up closed sections

Specimen ID	Slenderness ratio	EXP or FEA		AISI	σ_{EXP} or σ_{FEA} / σ_{AISI}
	L/r_{min}	σ_{EXP} or σ_{FEA} (N/mm^2)	Failure modes	σ_{AISI} (N/mm^2)	
BC40L440	25.35	257.71	L	242.28	1.06
BC40L840	48.40	236.32	L + F	219.95	1.07
BC40L1640	94.50	159.22	L + F	151.21	1.05
BC40L2240	129.08	96.34	F	97.28	0.99
BC50L440	25.76	255.18	L	242.60	1.05
BC50L840	49.19	235.00	L + F	219.54	1.07
BC50L1640	96.04	154.15	L + F	149.09	1.03
BC50L2240	131.18	96.63	F	94.46	1.02
BC60L440	26.17	259.43	L	242.87	1.07
BC60L840	49.96	233.79	L + F	219.10	1.07
BC60L1640	97.54	142.27	L + F	146.99	0.97
BC60L2240	133.22	89.81	F	91.84	0.98
TB30-I80-F50-L15-A45-440	26.93	254.40	L	233.31	1.09
TB30-I80-F50-L15-A45-840	51.41	227.62	L	211.23	1.08
TB30-I80-F50-L15-A45-1640	100.38	142.53	F	142.91	1.00
TB30-I80-F50-L15-A45-2240	137.10	89.66	F	87.13	1.03
TB30-I120-F50-L15-A45-440	28.32	203.66	L	207.45	0.98
TB30-I120-F50-L15-A45-840	54.06	197.04	L	186.55	1.06
TB30-I120-F50-L15-A45-1640	105.55	124.54	F	123.76	1.01
TB30-I120-F50-L15-A45-2240	144.16	78.43	F	77.41	1.01
TB40-I40-F50-L15-A45-440	24.47	268.85	L	244.25	1.10
TB40-I40-F50-L15-A45-840	46.71	250.21	D + F	223.22	1.12
TB40-I40-F50-L15-A45-1640	91.20	168.81	F	157.46	1.07
TB40-I40-F50-L15-A45-2240	124.27	108.26	F	104.56	1.04
TB50-I40-F50-L15-A45-440	23.79	266.74	L	245.81	1.09
TB50-I40-F50-L15-A45-840	45.42	251.06	D + F	225.75	1.11
TB50-I40-F50-L15-A45-1640	88.68	171.67	F	162.30	1.06
TB50-I40-F50-L15-A45-2240	121.12	111.46	F	110.21	1.01
TB60-I40-F50-L15-A45-440	23.26	263.43	L	237.55	1.11
TB60-I40-F50-L15-A45-840	44.40	250.85	L + F	221.46	1.13
TB60-I40-F50-L15-A45-1640	86.68	173.04	F	166.19	1.04
TB60-I40-F50-L15-A45-2240	118.40	113.21	F	114.80	0.99
TB80-I40-F50-L15-A45-440	22.46	254.10	L	217.29	1.17
TB80-I40-F50-L15-A45-840	42.89	242.97	L	204.00	1.19
TB80-I40-F50-L15-A45-1640	83.73	171.79	L + F	159.58	1.08
TB80-I40-F50-L15-A45-2240	114.36	113.41	F	118.99	0.95
TB120-I40-F50-L15-A45-440	21.49	182.88	L	179.39	1.02
TB120-I40-F50-L15-A45-840	41.02	177.34	L	169.78	1.04
TB120-I40-F50-L15-A45-1640	80.09	157.44	L + F	137.29	1.15
TB120-I40-F50-L15-A45-2240	109.39	104.38	L + F	107.08	0.97
TB30-I40-F40-L15-A45-440	33.11	262.13	L + F	233.67	1.12
TB30-I40-F40-L15-A45-840	63.21	229.63	F	198.16	1.16
TB30-I40-F40-L15-A45-1640	123.41	109.52	F	104.59	1.05
TB30-I40-F40-L15-A45-2240	168.56	65.13	F	56.96	1.14
TB30-I40-F80-L15-A45-440	14.87	253.62	L	220.88	1.15
TB30-I40-F80-L15-A45-840	28.40	245.86	L + D	214.50	1.15
TB30-I40-F80-L15-A45-1640	55.44	237.31	L + D	191.43	1.24

Table 4 (continued)

Specimen ID	Slenderness ratio	EXP or FEA		AISI	σ_{EXP} or σ_{FEA}
	L/r_{min}	σ_{EXP} or σ_{FEA} (N/mm^2)	Failure modes	σ_{AISI} (N/mm^2)	σ_{AISI}
TB30-I40-F80-L15-A45-2240	75.72	212.96	F	167.53	1.27
TB30-I40-F120-L15-A45-440	9.89	221.65	L	192.75	1.15
TB30-I40-F120-L15-A45-840	18.87	216.65	L	190.32	1.14
TB30-I40-F120-L15-A45-1640	36.85	213.27	L+D	181.18	1.18
TB30-I40-F120-L15-A45-2240	50.33	209.18	L+D	171.05	1.22
TB40-I40-F50-L10-A45-440	24.33	267.02	L+D	236.61	1.13
TB40-I40-F50-L10-A45-840	46.46	250.31	D+F	217.28	1.15
TB40-I40-F50-L10-A45-1640	90.70	169.85	F	156.10	1.09
TB40-I40-F50-L10-A45-2240	123.88	112.97	F	105.11	1.07
TB40-I40-F50-L30-A45-L440	24.89	266.35	L+D	238.59	1.12
TB40-I40-F50-L30-A45-L840	47.53	260.46	L+D	219.13	1.19
TB40-I40-F50-L30-A45-L1640	92.79	166.09	L+F	155.89	1.07
TB40-I40-F50-L30-A45-2240	126.74	109.61	F	102.42	1.07
TB30-I40-F50-L15-A30-L440	25.36	259.89	L+D	241.77	1.07
TB30-I40-F50-L15-A30-L840	49.07	233.36	D	219.48	1.06
TB30-I40-F50-L15-A30-L1640	97.37	164.28	F	150.86	1.09
TB30-I40-F50-L15-A30-2240	135.19	117.85	F	97.03	1.21
TB30-I40-F50-L15-A60-L440	25.39	268.71	L+D	243.35	1.10
TB30-I40-F50-L15-A60-L840	49.47	244.38	D	220.86	1.11
TB30-I40-F50-L15-A60-L1640	98.17	160.02	F	151.68	1.06
TB30-I40-F50-L15-A60-2240	136.33	101.42	F	97.45	1.04
TB30-I40-F50-L15-A80-L440	25.69	182.10	L	225.42	0.81
TB30-I40-F50-L15-A80-L840	49.67	163.83	L	207.13	0.79
TB30-I40-F50-L15-A80-L1640	98.57	132.44	F	148.87	0.89
TB30-I40-F50-L15-A80-2240	136.90	85.77	F	96.75	0.89
Mean					1.07
Coefficient of variation					0.081
Reliability index β					3.19

L local buckling, *D* distortional buckling, *F* flexural buckling

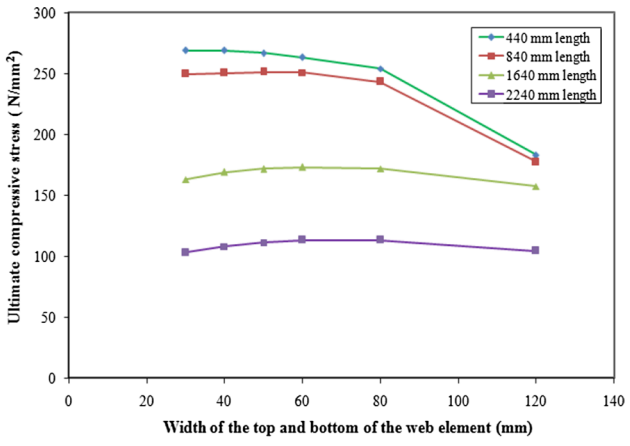

Fig. 16 Ultimate compressive stress vs. width of the top and bottom of the web element for the FEA specimens

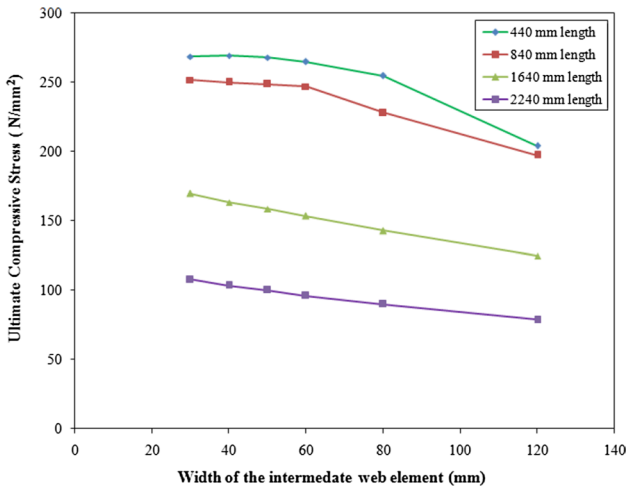

Fig. 17 Ultimate compressive stress vs. width of the intermediate web element for the FEA specimens

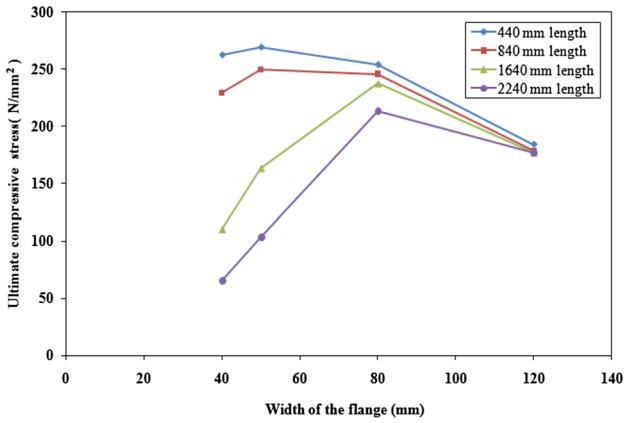

Fig. 18 Ultimate compressive stress vs. width of the flange for the FEA specimens

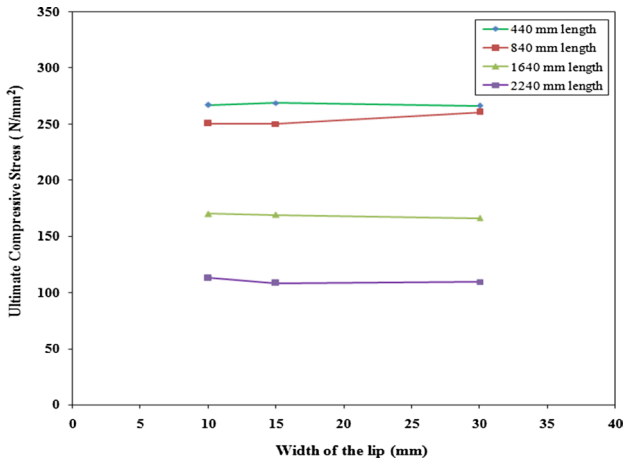

Fig. 19 Ultimate compressive stress vs. width of the lip for the FEA specimens

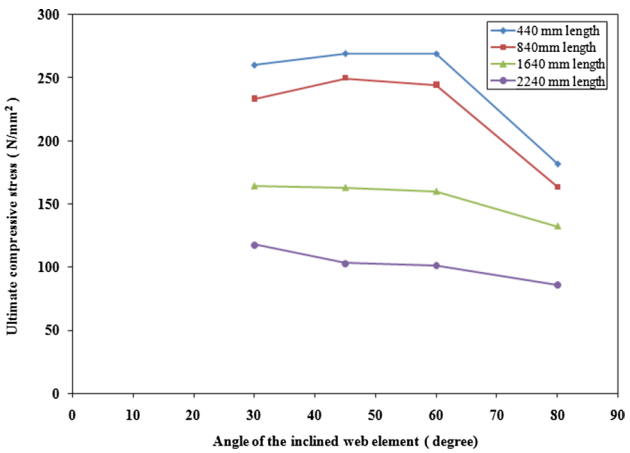

Fig. 20 Ultimate compressive stress vs. angle of the inclined web element for the FEA specimens

Conclusions

This paper describes strength and behaviour of cold-formed stiffened built-up closed sections with intermediate web stiffeners. Three series of test were conducted. Totally, 12 specimens were tested under the hinged end conditions. The accurate and reliable finite-element model was created using ANSYS. The ultimate compressive stress and failure modes obtained from the finite-element analysis were compared against those are obtained by the experiment. It was shown that FEA accurately predicts the capacity of the cold-formed built-up closed section with intermediate stiffeners. Therefore, the validated FEA model was used for the parametric study. Totally, 60 specimens were used for the parametric study to investigate the effect of all influential parameters such as width of the top and bottom of the web element, width of the intermediate web element and width of the flange, width of the lip, and angle of inclined web element. It is observed that the element with the lowest width-to-thickness ratio has more load-carrying capacity. The increase of width of lip and variation in angle of inclined element from 30° to 60° does not give any significant effects on the section. The results obtained from the parametric study were compared with the unfactored design strength calculated by the AISI specifications. The reliability of the AISI predictions was assessed by reliability analysis. It is shown that AISI predictions are conservative and reliable.

Compliance with ethical standards

Conflict of interest On behalf of all authors, the corresponding author states that there is no conflict of interest.

References

AISI-S100 (2007). *North American Specification for the Design of Cold-Formed Steel Structural members Specifications*.

American Institute of steel construction. AISC (2005). *Steel construction Manual*. Washington.

Aruna, G., Sukumar, S., & Karthika, V. (2015). Study on cold-formed steel built-up square sections with intermediate flange and web Stiffeners. *Asian Journal of Civil Engineering (BHRC), 16*(7), 919–931.

AS/NZS (2005). *Cold-formed steel structures*. Sydney, Australia: Australian/New Zealand Standard, AS/NZS 4600:2005, Standards Australia.

ASCE (2006). *Minimum design loads for buildings and other structures. ASCE/SEI 7-05*. American society of Civil Engineers Standard.

Dhanalakshmi, M., & Shanmugam, N. E. (2001). Design for openings in equal-angle cold-formed steel stub columns. *Thin-Walled Structures, 39,* 167–187.

Ellobody, E., & Young, B. (2005). Behavior of cold-formed steel plain angle columns. *Journal of Structural Engineering, 131*(3), 457–466.

Fratamico, D. C., Torabian, S., Zhao, X., Rasmussen, K. J. R., & Schafer, B. (2018). Experiments on the global buckling and collapse of built-up cold-formed steel columns. *Journal of Constructional Steel Research, 144,* 65–80.

Georgieva, I., Schueremans, L., & Pyl, L. (2012). Experimental investigation of built-up double–Z members in bending and compression. *Thin-Walled Structures, 53,* 48–57.

IS 1608: 2005 *(Part-I) Metallic materials—Tensile testing at ambient temperature*.

Li, Y., Li, Y., Wang, S., & Shen, Z. (2014). Ultimate load-carrying capacity of cold-formed thin walled columns with built-up box and I section under axial compression. *Thin-Walled Structures, 79,* 202–2017.

Narayanan, S., & Mahendran, M. (2003). Ultimate capacity of innovative cold-formed steel columns. *Journal of Constructional Steel Research, 59,* 489–508.

Piyawat, K., Ramseyer, C., & Kang, T. H.-K. (2013). Development of an axial load capacity equation for doubly symmetric built-up cold-formed sections. *Journal of Structural Engineering, American Society of Civil Engineers, 139*(12), 04013008.

Popovic, D., Hancock, G. J., & Rasmussen, J. R. (1999). Axial compression test of cold-formed angles. *Journal of Structural Engineering, 125*(5), 515–552.

Reyes, W., & Guzmanc, A. (2011). Evaluation of the slenderness ratio in built-up cold-formed box sections. *Journal of Constructional Steel Research, 67,* 929–935.

Roy, K., Mohammadjani, C., & Lim, B. P. (2018a). Experimental and numerical investigation into the behaviour of face-to-face built-up cold-formed steel channel sections under compression. *Thin-Walled Structures, 134,* 291–309.

Roy, K., Mohammadjani, C., & Lim, B. P. (2019). Experimental and numerical investigation into the behaviour of face-to-face built-up cold-formed steel channel sections under compression. *Thin-Walled Structures, 134,* 291–309.

Roy, K., Ting, T. C. H., Lau, H. H., & Lim, B. P. (2018b). Nonlinear behaviour of axially loaded back-to-back built-up cold-formed steel un-lipped channel sections. *Steel and Composite Structures, An International Journal, 28*(2), 233–250.

Roy, K., Ting, T. C. H., Lau, H. H., & Lim, B. P. (2018c). Nonlinear behaviour of back-to-back gapped built-up cold-formed steel channel sections under compression. *Journal of Constructional Steel Research, 147,* 257–276.

Schafer, B. E. (2002). Local, distortional, and euler buckling of thin-walled columns. *Journal of Structural Engineering, 128*(3), 288–299.

Schafer, B. W., & Pekoz, T. (1998). Computational modeling of cold-formed steel: characterizing geometric imperfections and residual stresses. *Journal of Constructional Steel Research, 47,* 193–210.

Stone, T. A., & Laboube, R. A. (2005). Behavior of cold-formed steel built-up I-sections. *Thin-Walled Structures, 43,* 185–1817.

Sukumar, S., Parameswaran, P., & Jayagopal, L. S. (2006). Local-, distortional- and euler-buckling of thin walled built-up open sections under compression. *Journal of Structural Engineering, SERC India, 32*(6), 447–454.

Ting, T. C. H., Roy, K., Lau, H. H., & Lim, B. P. (2017). Effect of screw spacing on behavior of axially loaded back-to-back cold formed steel built-up channel section. *Advances in Structural Engineering*. https://doi.org/10.1177/1369433217719986.

Whittle, J., & Ramseyer, C. (2009). Buckling capacities of axially loaded, cold-formed, built-up C-channels. *Thin-Walled Structures, 47,* 190–201.

Yan, J., & Young, B. (2002). Column test of cold-formed steel channels with complex stiffeners. *Journal of Structural Engineering, 128*(6), 737–745.

Young, B., & Chen, J. (2008a). Column test of cold-formed steel non-symmetric lipped angle sections. *Journal of Constructional Steel Research, 64,* 808–815.

Young, B., & Chen, J. (2008b). Design of cold-formed steel built-up closed sections with intermediate stiffeners. *Journal of Structural Engineering, 134*(5), 727–737.

Young, B., & Ellobody, E. (2007). Design of cold-formed steel unequal angle compression members. *Thin-Walled Structures, 45,* 330–338.

Young, B., & Hancock, G. J. (1992). Tests of cold-formed channels with local and distortional buckling. *Journal of Structural Engineering, 117*(7), 1789–1803.

Zhang, Y., Wang, C., & Zhang, Z. (2007). Tests and finite element analysis of pin-ended channel columns with inclined simple edge stiffeners. *Journal of Constructional Steel Research, 63,* 383–395.

Zhang, J., & Young, B. (2012). Compression tests of cold-formed steel I-shaped open sections with edge and web stiffeners. *Thin-Walled Structures, 52,* 1–11.